A Model for Calculating Desert Aerosol Turbidity over the Oceans from Geostationary Satellite Data

CARL C. NORTON, FREDERICK R. MOSHER, BARRY HINTON, DAVID W. MARTIN, DAVID SANTEK AND WILLIAM KUHLOW

Space Science and Engineering Center, University of Wisconsin, Madison 53706

(Manuscript received 10 December 1979, in final form 1 March 1980)

ABSTRACT

A technique has been developed to infer the optical thickness of Saharan dust from Synchronous Meteorological Satellite (SMS) brightness measurements at visible wavelengths. The scattering model consists of an air layer, a dust layer and a lower boundary of variable albedo. Single-scatter properties of the dust computed from Mie theory were the basis for calculations by plane-parallel theory of radiative transfer in the dust layer. Radiative interactions between air and dust layers and the lower boundary were calculated with an adding version of the doubling scheme. Optical thickness was determined from satellite brightness measurements through a lookup table produced by the adding program. SMS visible sensors were calibrated from the prelaunch calibration measurements and measurements of sun and space. Error analysis and tests indicate a potential accuracy of ~0.1 unit of optical thickness. The main limits on accuracy are digitizing resolution of the SMS visible signals, and mistaking clouds for dust in the satellite imagery. This technique of inferring Saharan dust turbidity has been verified and fine-tuned using surface turbidity measurements during GATE and corresponding SMS imagery.

1. Introduction

One of the most spectacular events viewed on summertime satellite photographs of the tropical North Atlantic Ocean is the westward migration of clouds of Saharan dust. The three-dimensional characteristics and life cycle of these dust clouds have been described by Carlson and Prospero (1972), Carlson (1979) and Prospero (1979). The dust is imbedded in Saharan air layers in the middle troposphere. Its formation and movement are closely coupled to African waves. Dust is thought to have important effects on the radiation balance of the tropical North Atlantic (Carlson and Prospero, 1977;[1] Carlson, 1979; Carlson and Benjamin, 1980) and, in conjunction with Saharan air, on the formation and organization of clouds (Carlson and Prospero, 1972; Carlson, 1979; Martin and Sikdar, 1975, 1979). Indeed, measurements of dust formed an important subprogram of the GARP Atlantic Tropical Experiment (GATE) conducted in 1974 (Prospero *et al.*, 1976a,b).[2,3]

Although the GATE dust turbidity measurements are the most extensive available, they consist of only a dozen land and ship stations, mostly concentrated in the eastern Atlantic. In addition these measurements are available only for the summer months of 1974. Synoptic-scale analyses of these data require an active imagination. It is the sparsity of surface observing stations across the tropical Atlantic that makes satellite data an obvious choice in the development of new dust turbidity measurement techniques.

One can infer turbidity due to aerosols such as dust by relating observed intensities of radiation returned from the earth-atmosphere system to the radiation expected from an atmosphere containing a dust layer of specified optical thickness (τ; base e). Geostationary satellite data, after calibration, provide the observed intensities. The expected radiation from an earth-atmosphere system of any desired τ is then calculated from radiative transfer programs.

A number of difficulties arise, however, when one attempts to apply this conceptually simple scheme. First, geostationary satellite visible sensor response is such that dust can best be detected over dark backgrounds such as the oceans. Next, efforts to obtain clear-sky radiances are hampered by cloud contamination, signal noise and sensor calibration errors. Finally, the optical characteristics and physical properties of the dust must be determined or approximated.

[1] Carlson, T. N., and J. M. Prospero, 1977: Saharan air outbreaks: Meteorology, aerosols, and radiation. Report of the U.S. GATE Central Program Workshop, 57–78.

[2] Prospero, J. M., T. N. Carlson, D. Savoie and R. T. Nees, 1976a: Atmospheric turbidity measurements during GATE. Tech. Rep. No. TR 76-6, University of Miami, GATE data archives.

[3] Prospero, J. M., R. T. Nees and D. Savoie, 1976b: Atmospheric aerosol measurements during GATE. Tech. Rep. No. TR 76-5, University of Miami, GATE data archives.

0021-8952/80/060633-12$07.00

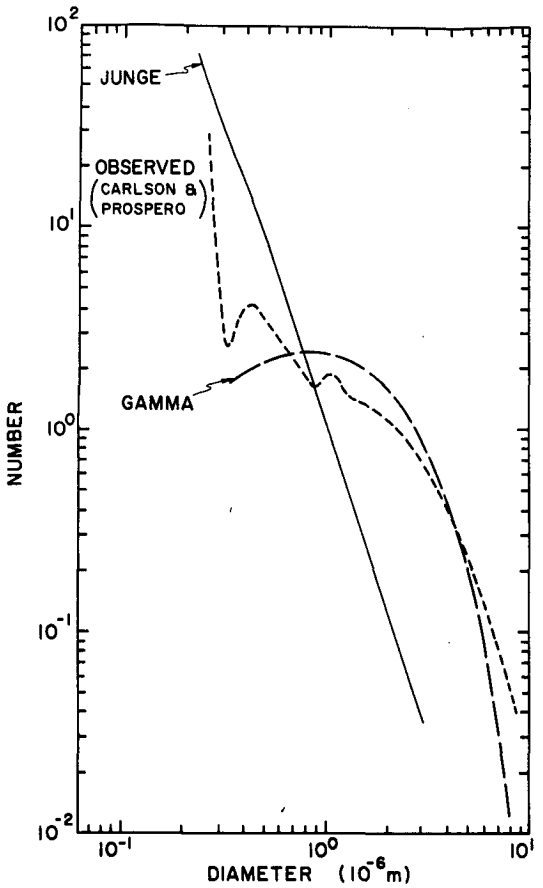

FIG. 1. Comparison of Junge, gamma and observed dust particle size distributions.

In developing our turbidity measurement technique we examined SMS 1 imagery from the GATE period. Numerous determinations of satellite perceived brightness values were made of apparently cloud-free dusty areas to compare our turbidity results with surface based observations. These satellite brightness values were related to the theoretical values produced by a doubling program of Hansen (1971). The layered character of the Saharan dust makes the plane parallel doubling routine especially attractive, although other radiative transfer programs may be used (e.g., Carlson, 1979). Computation of the single-scatter properties of air and dust was the first step in the radiative transfer calculation process.

2. The single-scatter program

Phase functions and single-scatter albedoes were computed from a Mie scatter program provided by J. E. Hansen. This program is an efficient scheme for the computation of single scattering for a specified particle size distribution of homogeneous spherical particles.[4] Input requirements are mean particle radius, size distribution, wavelength of incident radiation and complex refractive index. In its original form the routine contained several common theoretical size distributions, including log-normal, level, gamma and Deirmendjian. We added the capability of making computations using observed size distributions.

The Mie scatter program was run for air molecules as a check of the validity of the procedures. The refractive index used was a weighted mean of the indices of the three most abundant atmospheric constituents (oxygen, nitrogen and argon). A size distribution was determined from physical data found in the *Handbook of Chemistry and Physics* (1960). The phase function produced by the routine was indistinguishable from the analytical solution for Rayleigh scattering. The computed single-scatter albedo $\tilde{\omega}$ was unity.

3. Dust scattering phase function

The dust particle size distribution used in the Mie scatter program was based on data collected by Carlson and Prospero (1977)[1] during GATE (Fig. 1). The gamma distribution used to approximate the observed distribution is

$$n(r) = r^{(1-3b)/b} \exp(-r/ab), \qquad (1)$$

where $n(r)$ is number of particles of radius r, a the effective radius and b the effective variance. The Carlson and Prospero data are approximated by 2.06 for a and 0.26 for b. Phase functions and single-scatter albedos produced by the observed and gamma distributions are compared in Fig. 2. Intensities calculated from these distributions were not significantly different. The parameterized distribution given by (1) was used in all subsequent computations.

A complex refractive index for Saharan dust was selected after examining values measured by several investigators (Table 1). A sensitivity study showed that when extreme values were used, the output intensities varied by less than 3% for $\tau = 0.125$ but by as much as 34% for $\tau = 4.0$. Fig. 3 shows the phase functions and single-scatter albedoes produced from computations using three indices. The complex refractive index chosen for all Mie scatter calculations was $1.56-0.0053i$. Single-scatter properties of air and dust were computed for a wavelength (0.65 μm) approximating the mean of the SMS 1 visible sensor response range. These parameters were required to

[4] Chýlek *et al.* (1976) developed a modification of Mie's solution which is applicable for randomly oriented arbitrarily shaped non-spherical particles.

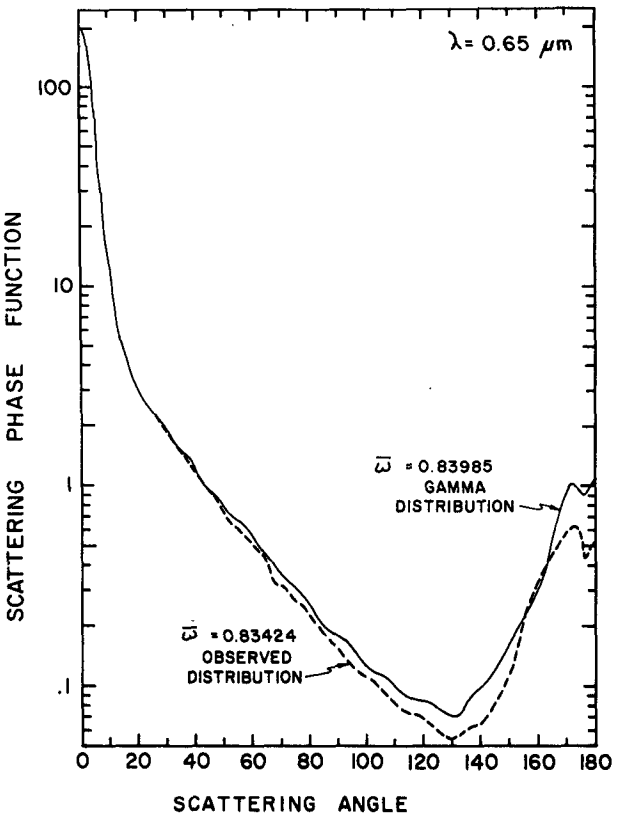

FIG. 2. Phase functions resulting from gamma and observed particle size distributions.

treat the general case of radiative transfer in the air-dust layer.

4. Multiple scattering

Multiple scattering was computed from a modified version of a doubling program provided by J. E. Hansen. The doubling process begins with a homogeneous layer of such small optical thickness that the radiation exiting the top and bottom is the product of only single-scattering events as calculated from the Mie scatter routine. Doubling the very thin layer quickly produces a layer of any desired optical thickness (Hansen, 1971).

Since the doubling process is valid only for homogeneous layers, it was necessary to modify the program to produce an "adding" routine. This allows computations of the radiative interactions between the air and dust layers and with the lower surface.

Input parameters for the doubling program were single-scatter albedoes, phase functions, number of quadrature points for the Gaussian integration, optical thickness desired, azimuth angles (ϕ) and surface albedo (A). The solar zenith angles (θ_0) and satellite viewing angles (θ) were those used in the Gaussian integration (7.8°, 17.8°, 27.8°, 37.5°, 46.8°, 55.8°, 64.1°, 71.6°, 78.1°, 83.4°, 87.3°, 89.5°). Azimuth angles ranged from 0–150° in 30° increments.

TABLE 1. Refractive index.

	Real	Imaginary
Carlson and Prospero (1977)[a,1]		
Mica (50%)	1.561	—
Quartz (14–20%)	1.544	—
Kaolinite (6–7%)	1.565	—
Carlson and Caverly (1977)[a]	1.54	0.0025
Grams *et al.* (1974)[a]	1.525	0.0055
Patterson *et al.* (1977)[a]	1.558	0.0038
Lindberg *et al.* (1976)[b,6]	—	0.0053

[a] Saharan dust, [b]Negev dust.

Sea surface reflectivities used for the lower boundary were inferred from the albedo measurements of Payne (1972) with the contributions due to the direct (specularly reflected) beam subtracted from his values. This was necessary because the satellite sensor detects a bidirectional reflectance rather than

[6] Lindberg, J. D., J. B. Gillespie and B. Hinds, 1976: Paper presented at the Symposium on Radiation in the Atmosphere. Int. Assoc. Meteor. Atmos. Phys., Garmisch-Partenkirchen, West Germany.

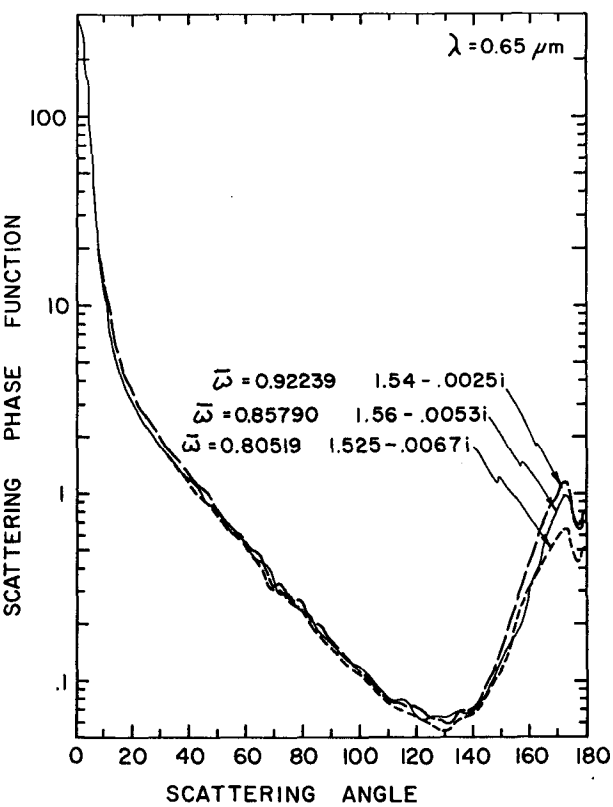

FIG. 3. Phase functions and single-scatter albedoes computed from three refractive indices.

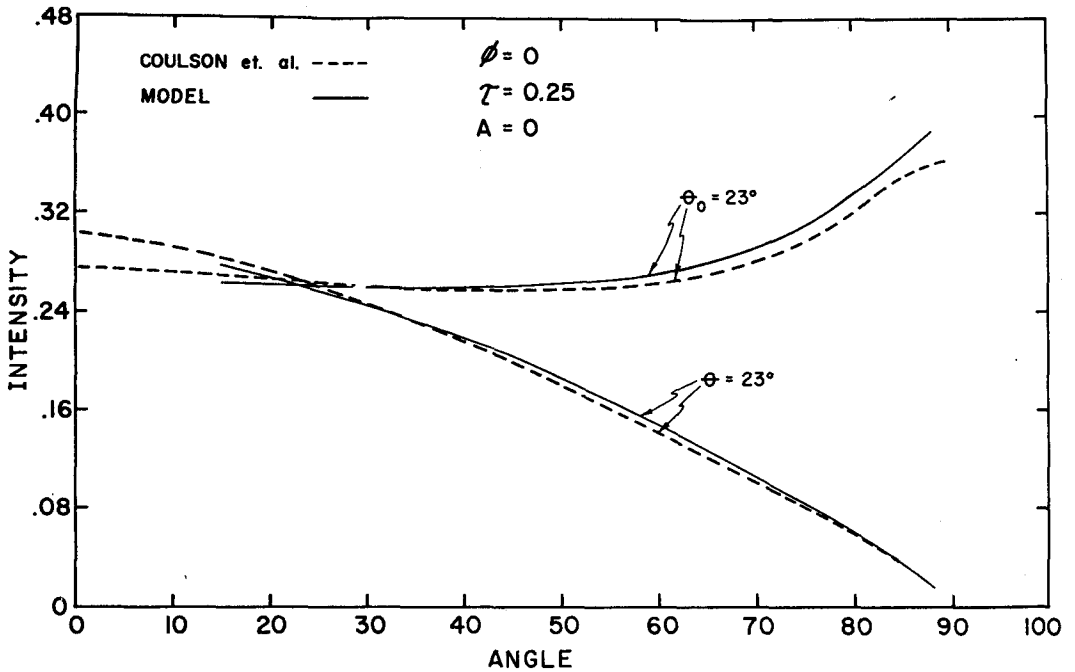

FIG. 4. Comparison of multiple-scatter (doubling) intensities with Coulson *et al.*'s table for an air layer of 0.25 optical thickness and surface albedo of zero.

a hemispheric albedo. Use of the model near-sun glint is therefore precluded.

Although Payne states that there is no discernable effect on the sea surface albedo from wind or whitecaps, it was desirable to further investigate this point. A semi-theoretical technique developed by Burt (1954) considers the distribution of slope on the sea surface to relate albedo to wind speed. For light winds and clear skies, agreement with Payne's table was within 10%. Agreement was within 20% for $\theta_0 = 70°$ and wind speeds up to 15 m s^{-1}.

Monahan (1971) reported a 7.6% whitecap coverage for a 17.5 m s^{-1} wind. If we use 0.06 for the sea albedo and 0.40 for the whitecap albedo (Lauscher, 1955), we find a 43% increase in the sea surface albedo when whitecaps are included. An SMS 1 sensitivity study showed that a 50% change in the sea surface albedo would produce a one or two bit digital count error for θ_0 of 0–45° and τ of 0.25. An error of four digital counts would occur for large (75°) θ_0 and small (0.0625) τ. One or two digital counts correspond to 10–20% error in the observed sea surface count. This is approximately the same as the uncertainty inherent in the sea surface brightness observations. In addition, further tests show that as τ increased beyond 0.50, a 50% error in sea surface albedo was not detectable in the radiation intensity exiting the top of the atmosphere. Thus over typical ranges of surface wind speed and scene geometry the error contributed by wind (outside areas of sunglint) is negligibly small.

In order to examine the accuracy of the doubling routine results, several test runs were made for air layers. Fig. 4 shows close agreement between our computed intensities of radiation exiting the top of the atmosphere and those of Coulson *et al.* (1960) for a lower albedo of zero. Fig. 5 is a similar comparison for a surface albedo of 0.25.

Next, the adding routine was tested using two identical air layers of $\tau = 0.25$ to produce a single air layer of $\tau = 0.50$. Fig. 6 is a comparison of this result with Coulson's values for $\tau = 0.50$. Finally, Fig. 7 compares the results of reversal of the dust-air layer in the adding routine. Intensities differ by less than 5% over a θ and θ_0 range of 15–75°. The successful completion of these tests encourages confidence in the results of the computations.

The multiple-scattering programs were then used to compute a table of intensities as functions of τ, θ, θ_0 and ϕ for the appropriate sea surface albedoes. Values of τ ranged from 0.0625 to 8.0000. The smallest τ was determined to be a reasonable value for the optical thickness of a clear atmosphere for the SMS 1 sensor response range. Dust layers of optical thicknesses ranging from 0.0000 to 7.9375 were added to the clear atmosphere values to give total atmospheric optical thicknesses of 0.0625, 0.125, 0.25, 0.50, 1.0, 2.0, 4.0 and 8.0. The table of $I = f(\tau,\theta,\theta_0,\phi)$

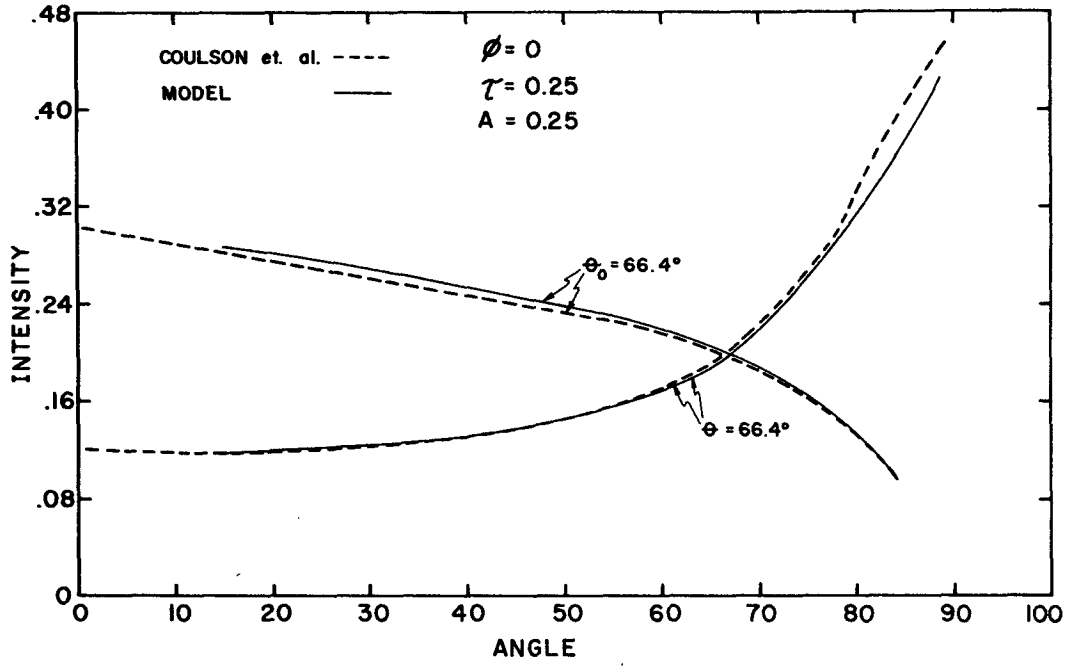

FIG. 5. As in Fig. 4 except for a different satellite-solar zenith angles and for an albedo of 0.25.

was inverted to produce a lookup table of $\tau = f(I,\theta, \theta_0,\phi)$. This table was then installed on the Space Science and Engineering Center's Man-Computer Interactive Data Access System, McIDAS (Chatters and Suomi, 1975).

5. Calibration

In order to relate the satellite observed intensities to those stored in the lookup table, it was necessary to calibrate the sensors either absolutely or relative

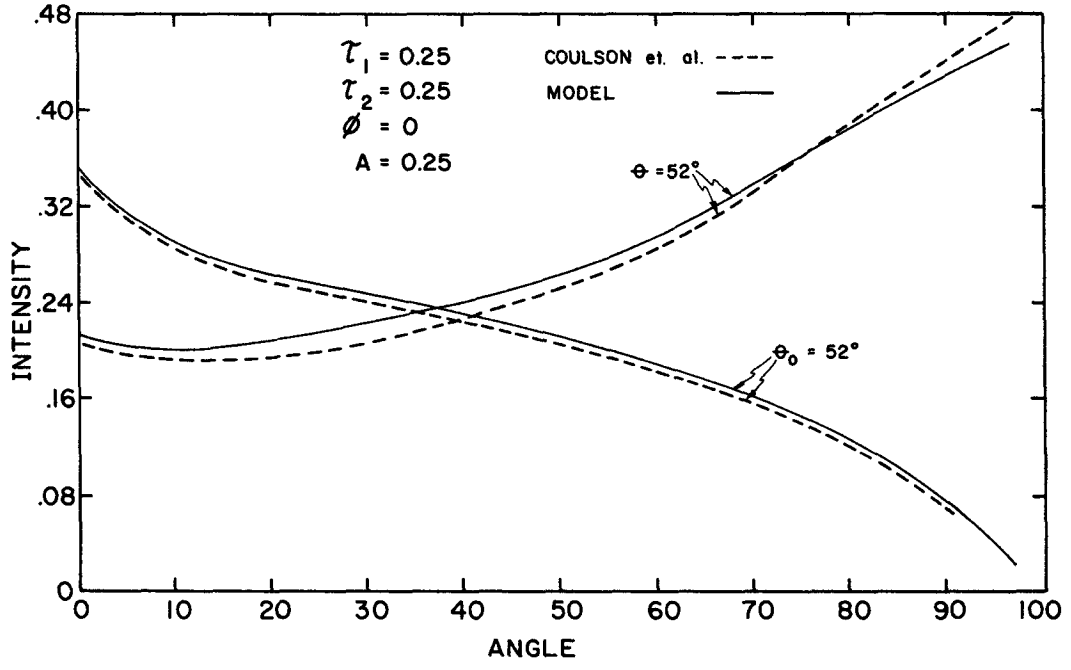

FIG. 6. Comparison of multiple-scatter (adding) intensities with Coulson *et al.*'s table for two air layers of optical thickness 0.25 and an albedo of 0.25.

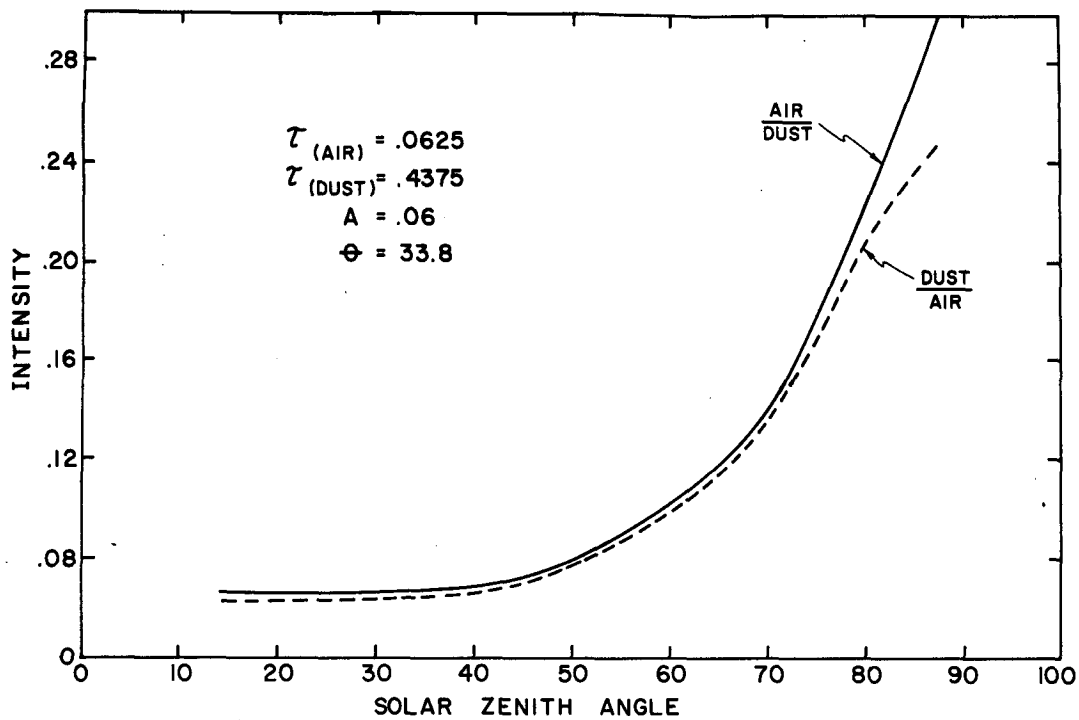

FIG. 7. Comparison of the effect of reversing the air-dust layering in the multiple-scatter (adding) routine.

to a reference standard. We choose the latter since our model is based on reflectivity measurements. Smith and Loranger (1977)[5] performed an absolute calibration for a different application. If we assume the prelaunch reflectance of the reference target remained unchanged, then our results and Smith's agree quite well. The Appendix gives a description of the calibration process.

6. Error analysis

Satellite brightness measurements are subject to several sources of error. There are errors associated with the instrument and errors associated with the recording and storing of the data. Instrumental errors are introduced by random noise in the signal, digitization round-off and calibration errors. If we examine a large number of samples from a given sensor of a target of constant reflectivity, the spread of the digital counts (ΔCT) is a measure of the first two instrumental errors combined. From data similar to that given in the Appendix, we find that ΔCT is less than 1.

Errors due to drift of the sensor calibration can be determined from two independent determinations of calibration. We found that for the range of digital counts useful for dust determinations, there was a 5% error in radiance due to ignoring the drift of the eight sensor offsets over a 3-week period. There was also an error of less than 2% due to the drift in the coefficient of variation of sensor output with radiance over the same period.

Since these drift errors can be controlled by more frequent calibration, the most significant error (E) is due to digitization and noise. For a given data point (pixel) this is the order of

$$E = 2\Delta\mathrm{CT}/\mathrm{CT}. \tag{2}$$

In (2) the digital count (CT) ranges from zero to 63. For the oceans CT is about 11. The factor of 2 arises from the squaring of CT to obtain radiance. Thus, for a single pixel E is less than 20% over the ocean. If, however, n-independent pixels are used to determine a representative value of CT, then E can be estimated by

$$E = 2\Delta\mathrm{CT}/\sqrt{n}\mathrm{CT}. \tag{3}$$

Typically n is about 100, therefore E is ~2%. As a worst case estimate we can take $n \approx 4$ and use the 3-week change in calibration as the characteristic calibration error. From the more complete expression for the error in reflectivity (or normalized intensity) derived in the Appendix, we find that the uncertainty in reflectivity ranges from <0.01 for very low reflectivity to ~0.015 for reflectivities the order of 0.12. Thus, over the range of interest the uncertainty in reflectivity is ~10%. With the help of information like that shown in Fig. 8 we can translate

[5] Smith, E. A., and D. Loranger, 1977: Radiometric calibration of polar and geosynchronous satellite shortwave detectors for albedo measurements. Dept. Atmos. Sci., Colorado State University, Fort Collins (unpublished manuscript).

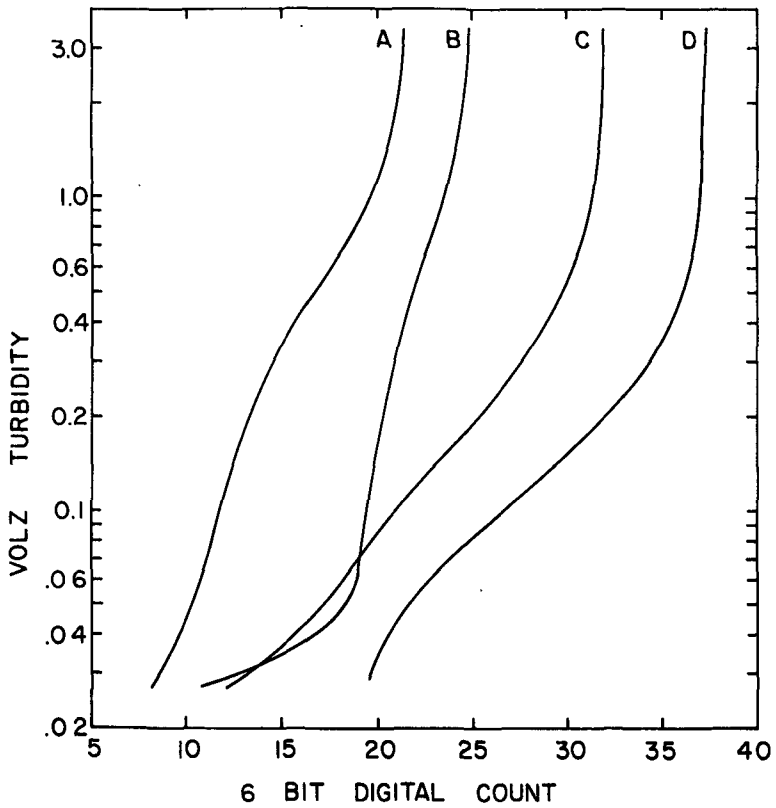

FIG. 8. Error sensitivity curves for several values of θ_0/θ: curve A = 18°/18°, curve B = 18°/64°, curve C = 64°/64°, curve D = 72°/72°.

the uncertainty in reflectivity or digital count into an uncertainty of optical thickness or Volz turbidity.

Erroneous digital values due to archive errors appear on displayed images as garbled scan lines or salt and pepper noise. Typically much less than 10% of the image is affected so that measurements can be made in noise-free areas. Alternatively, measurements can be made in noisy areas after filtering noise spikes.

7. Measuring turbidity

Except in one respect, the measurement of turbidity is straightforward. The exception is selection of a representative digital count. This requires the judgment of a meteorologist, for the problems are substantial. As discussed in Section 7 there is some uncertainty inherent in the data; but a more serious problem is distinguishing between cloud and dust (see Carlson, 1979, p. 334). Here we may be dealing with small clouds (primarily trade cumulus) which do not fill the sensor field of view or thin clouds of optical thickness comparable to that of dust. The problem of small clouds is handled by selecting digital counts from images of the highest practical resolution, usually 1 or 2 km, over apparently cloud-free areas of at least 15 lines and elements. Although small clouds may be present in the image, the probability is high that at least one pixel (field of view) will be free of clouds.

Thin clouds, particularly cirrus, often can be detected on the matching infrared (IR) picture. If the question of thin cirrus is not resolved by the IR image, a final test is viewing a sequence of visible and IR images. Thin cirrus "ghosts" are apparent as subtle changes in texture which move across the face of the television screen. Thin altostratus or altocumulus may be identified by rapid change in form, texture, and real or apparent motion.

After these considerations a representative digital count is selected from a frequency distribution of digital count for each sensor for the selected area. Several schemes were tested for selecting the best digital count from the histograms. The most consistent results, given the noise characteristics of the data and possibilities of cloud contamination, were obtained by taking the lowest value contiguous to the main peak of the distribution, or a value somewhat higher if the distribution had a long tail. Carlson (1979) and Carlson and Wendling (1977) followed a similar procedure.

Entering the selected digital count and sensor number on McIDAS causes three things to happen: digital count is converted to intensity via the calibration process previously referred to; θ, θ_0, ϕ are cal-

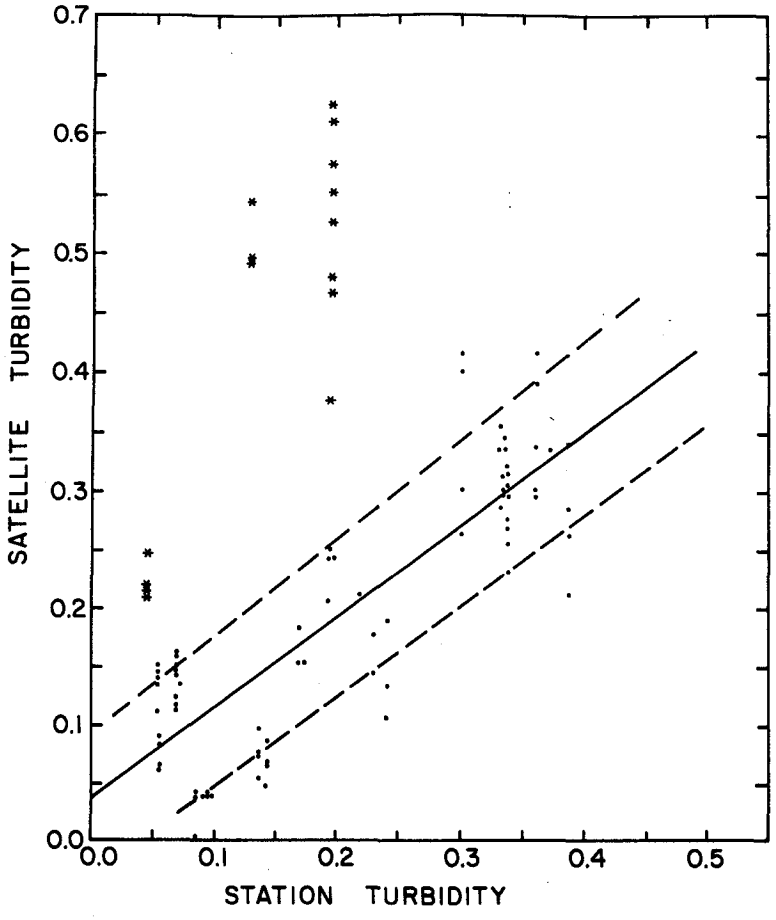

FIG. 9. Scatter diagram of satellite inferred turbidity and surface measured turbidity. Points found (in subsequent analysis) to be contaminated by clouds are marked with an asterisk. The solid line is the least squares linear regression line fitted to cloud free points.

culated through a satellite-to-earth coordinate transformation program (described by Smith and Phillips (1972); and τ is interpolated from the lookup table and converted to Volz turbidity.

8. Results

Eighty-nine histograms of digital count were examined. These data were extracted from the GATE SMS 1 archive and were selected to correspond closely in time and space to the turbidity measurements made by land stations and ships. Differences were not more than 2 h in time or 150 km in distance.

Fig. 9 shows the relationship between satellite and surface turbidity measurements. For the initial determination of satellite turbidity only a single visible image was used to select the representative digital count. A second look at the data using IR images and a time sequence revealed several cases of cloud contamination (denoted by asterisks) that were not apparent on a single visible image. Correlation of the total set of satellite and ground turbidity measurements is 0.44. Exclusion of the cloud-contaminated points results in a 0.85 correlation. The standard error of estimate (denoted by dashed lines) is 0.06. Fig. 10 is an example of an analysis made from satellite inferred turbidity measurements. A single experimental mapping gave ~30 values distributed across the Atlantic, and a plausible pattern of Saharan dust.

9. Conclusions

We have shown how geostationary satellite data can be used in conjunction with a plane parallel radiative transfer routine to estimate the optical thickness of Saharan dust over the tropical Atlantic. The theoretical curves of Fig. 8 show that measurements of Volz turbidity are possible to an accuracy of 0.1 up to values of ~0.8. Preliminary verification of our model (Fig. 9) demonstrates the achievement of this accuracy up to Volz turbidity values of 0.4. Although the 0.85 correlation coefficient is very

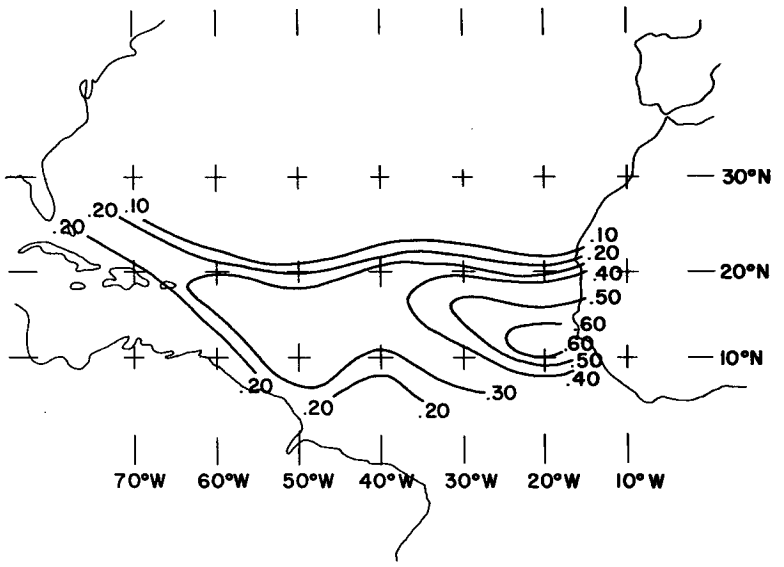

FIG. 10. An analysis of the satellite inferred turbidity field for 1500 GMT 27 June 1974.

encouraging, there is an obvious need for additional comparisons at larger values.

The present turbidity model is designed to work only over relatively large bodies of water. Aerosol turbidity measurement over land is a considerably more difficult problem because the reflectivity of the land surface may approximate that of the dust and the land albedo can vary dramatically in both space and time. We expect that the model in its current form will provide information which in conjunction with surface observations will be useful in studies of radiative heating and cooling of Saharan dust layers, relationship of dust with Saharan air, African waves and tropical convection.

APPENDIX

Sensor Calibration

The SMS/GOES spacecraft constructs an earth image by scanning an optical telescope. East–west scanning is accomplished by the spin of the spacecraft, while north–south scanning is accomplished by an array of eight detectors and a plane mirror whose angle is stepped mechanically. A small portion of the telescope entrance aperture is occluded by three very small dove prisms which reflect into the main optical path light arriving from different fields of view. Thus the image we recover is a multiple exposure or superposition of several fields of view. Usually the fields of view of the prisms will be either earth scenes or the blackness of space. Because of the extremely small apertures of each prism relative to the main image path, the secondary images of earth scenes or space are totally negligible relative to the primary image.

However, in the event that the prism field of view includes the sun, which is orders of magnitude brighter than earth scenes or space, the solar image due to the prism will be a prominent feature in the combined image. The sun is seen by the prisms only when it is beyond the earth, near midnight at the subsatellite point. At these times the earth, as seen by the satellite, is dark except perhaps for a rim or crescent of direct illumination and light scattered by the atmosphere. Thus, a portion of the image consists of the sun reflected by the prism on a black background. This solar image is then a reference object for relative calibration. A second reference point is black, either the dark side of the earth (at midnight) or space. The second reference is required because of the possibility of dark current from the

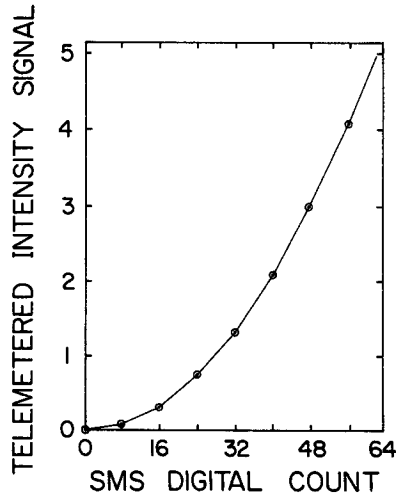

FIG. A1. Digital count signal intensity transfer function.

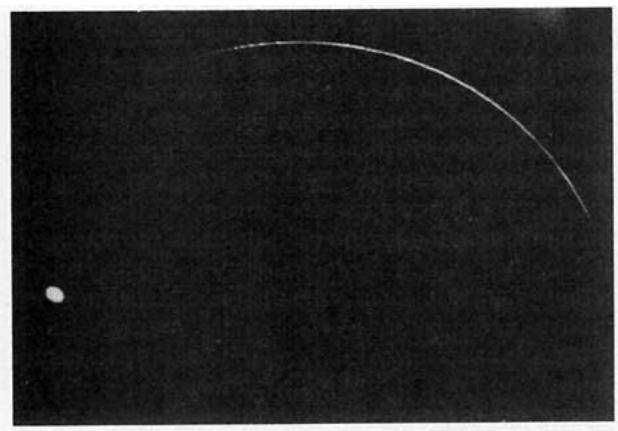

FIG. A2. SMS 1 earth image recorded near midnight at the subsatellite point. The white oval in the lower left is the reflected sun image.

photomultipliers or zero offsets in the signal conditioning circuitry.

According to the idealized data encoding scheme, "black" would be assigned a digital value of 0, while "white" (the intensity received from a Lambertian surface of 100% reflectance under full solar illumination) is assigned the value 63. Intermediate values follow a ½ power function, i.e.,

$$\mathrm{CT} = 63R^{1/2}. \tag{A1}$$

In the above equation CT is the digital count value and R the equivalent reflectance. It follows from (A1) that intensities should be proportional to CT-squared [Eq. (A2)]. Thus in the ideal case $(\mathrm{CT})^2$ is linearly related to the photomultiplier signal current I for each detector:

$$(\mathrm{CT})^2_{\mathrm{IDEAL}} = (63)^2 I/I_{\mathrm{WHITE}}. \tag{A2}$$

In actuality we find differences among the eight individual detectors, and small offsets of the digital values. This suggests a model for each of the (i = 1, . . . , 8) detectors of the form

$$I/I_{\mathrm{WHITE}} = B(i)[\mathrm{CT}(i)^2 - A(i)] \tag{A3}$$

or, in terms of reflectivity R,

$$R = B(i)[\mathrm{CT}(i)^2 - A(i)]. \tag{A4}$$

The coefficients $A(i)$ and $B(i)$ are found by insert-

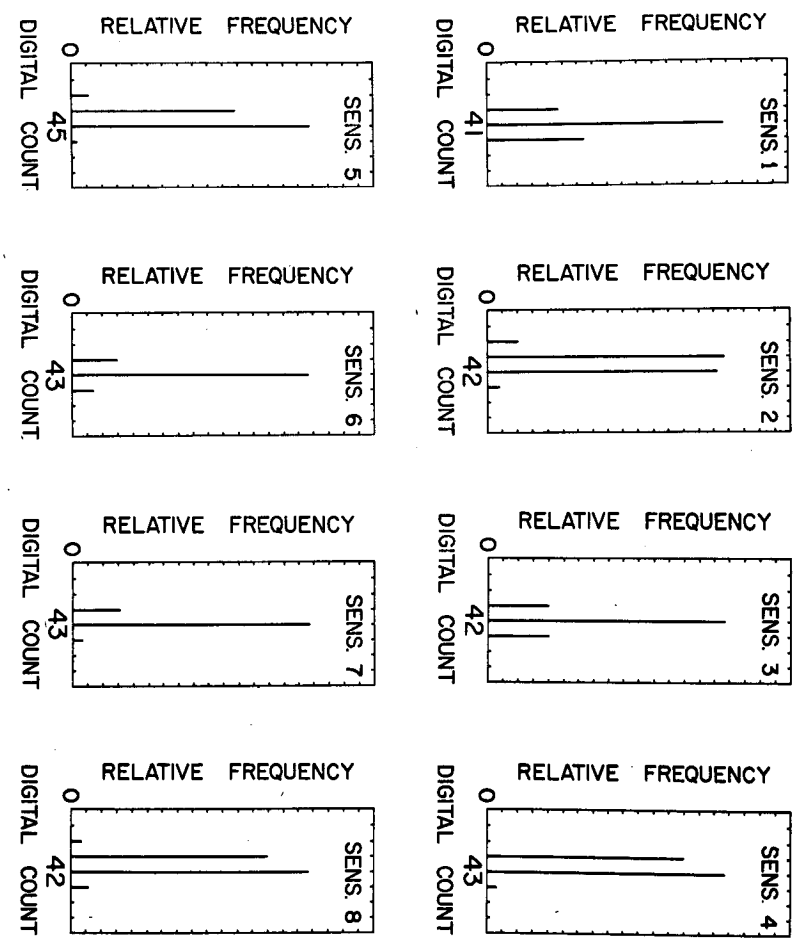

FIG. A3. Distribution of digital values for each sensor in the solar image.

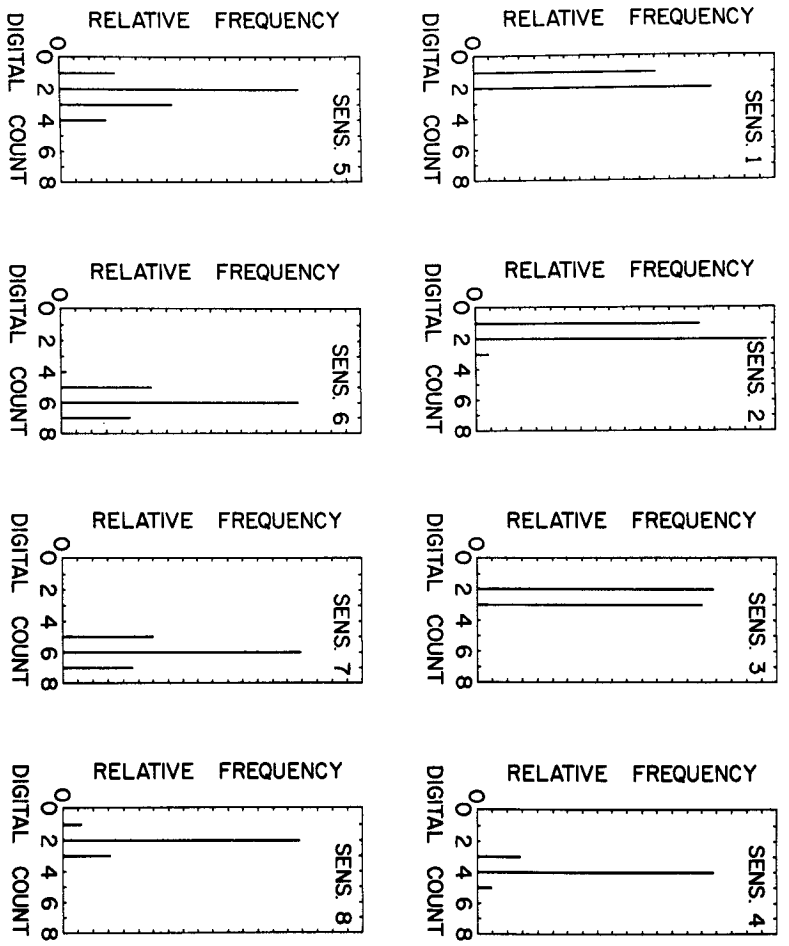

FIG. A4. As in A3 except for the "black" area of Fig. A2.

ing the observed values of CT(i) obtained for space (corresponding to $R = 0$) and the reflected solar images discussed above. In the latter case R was assumed equal to the preflight values of "equivalent prism reflectivity" (~0.48).

Because each $B(i) \approx 1$ and the offsets $A(i)$ are all small relative to $0.5(63)^2$, the determination of the $A(i)$'s and $B(i)$'s are practically independent of each other. If $\Delta A(i)$ is the error in $A(i)$, $\Delta B(i)$ the error in $B(i)$ and ΔCT the digitization and noise error, Eq. (A5) describes ΔR, the error of reflectivity:

$$\Delta R = R\Delta B(i) = B(i)\Delta A(i) + 2B(i)\mathrm{CT}\Delta\mathrm{CT}. \quad \text{(A5)}$$

TABLE A1. Calibration parameters.

Sensor*	A	B
0	2.0	1.039
1	1.4	1.107
2	2.9	1.085
3	2.1	1.057
4	3.9	1.070
5	1.6	0.984
6	4.0	1.032
7	4.1	1.032

* Sensor number is the remainder from dividing image line number by 8. This designation does not correspond to the manufacturer's assignment of sensor number, but it is self-consistent and more convenient for image users.

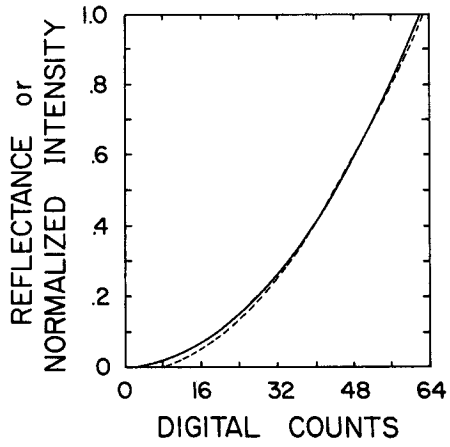

FIG. A5. Calibration comparison. The dashed curve is from Smith and Loranger (1977).

We found that for reflectivities ≥ 0.1 the $A(i)$'s are utterly negligible. Note that it makes little difference in (A5) if $B(i)$ is replaced by unity. Strictly speaking, the functional relation of photocurrent and count values does not quite follow simple analytical relations as assumed above. The actual relation is determined by an electrical curve fitting circuit whose response is illustrated in Fig. A1. Though this transfer function must be (and was) taken into account, it somewhat complicates the discussion of the calibration process.

Fig. A2 shows an image of the earth made just after midnight at the subsatellite point. Fig. A3 shows the distributions of digital values for each sensor in the solar image. Fig. A4 shows the distributions of digital values corresponding to the "black" area of Fig. 9. From these and similar figures one obtains estimates of the $A(i)$ and $B(i)$ according to (A4).

Table A1 shows the A and B values obtained for September 1974. Because of changes in the earth-sun distance and potential drifts in the photomultiplier characteristics these values may not apply at other times. In particular it is now the practice of the National Environmental Satellite Service to apply a transformation to the data for the purpose of reducing the aesthetically displeasing stripes which arise from differences among detectors. This transformation is derived statistically from an analysis of a sample image by constraining the digital signals of each detector to agree with a key detector, or to the average response of all detectors in those parts of the image which seem to have broad areas of uniform reflectance. If this transformation is known, its inverse can be generated, and the original counts restored, but with increased round-off errors. Such a cosmetic transformation was not applied to the data considered in the present paper.

Eq. (A4) can be averaged over the eight sensors and the results compared to the results of Smith and Loranger (1977) mentioned previously. As shown in Fig. A5 the agreement is quite good—except possibly for the portion of the scale below CT = 10. However, Smith and Loranger essentially performed the calibration by transferring the calibration of NOAA 2 to SMS 1 by intercomparison of common targets. Since the natural scenes used contained few or no targets corresponding to SMS counts less than 10, it is not surprising that the curves would disagree here.

REFERENCES

Burt, W. V., 1954: Albedo over wind-roughened water. *J. Meteor.*, **11**, 283–290.

Carlson, T. N., 1979: Atmospheric turbidity in Saharan dust outbreaks as determined by analyses of satellite brightness data. *Mon. Wea. Rev.*, **107**, 322–335.

——, and J. M. Prospero, 1972: The large-scale movement of Saharan air outbreaks over the northern equatorial Atlantic. *J. Appl. Meteor.*, **11**, 283–297.

——, and R. S. Caverly, 1977: Radiative characteristics of Saharan dust at solar wavelengths. *J. Geophys. Res.*, **82**, 3141–3151.

——, and P. Wendling, 1977: Reflected radiance measured by NOAA 3 VHHR as a function of optical depth for Saharan dust. *J. Appl. Meteor.*, **16**, 1368–1371.

——, and S. G. Benjamin, 1980: Radiative heating rates for Saharan dust. *J. Atmos. Sci.*, **37**, 193–213.

Chatters, G. C., and V. E. Suomi, 1975: The application of McIDAS. *IEEE Trans. Geosci. Electron.*, **GE-13**, 137–146.

Chýlek, P., G. W. Grams and R. G. Pinnick, 1976: Light scattering by irregular randomly oriented particles. *Science*, **193**, 480–482.

Coulson, K. L., J. V. Dave and Z. Sekera, 1960: *Tables Related to Radiation Emerging from a Planetary Atmosphere with Rayleigh Scattering.* University of California Press, Berkeley, 584 pp.

Grams, G. W., J. H. Blifford, Jr., D. A. Gillette and P. B. Russell, 1974: Complex index of refraction of airborne soil particles. *J. Appl. Meteor.*, **13**, 459–471.

Hansen, J. E., 1971: Multiple scattering of polarized light in planetary atmospheres: I. The doubling method. *J. Atmos. Sci.*, **28**, 120.

Lauscher, P., 1955: Sonnen und Himmelstrahlung in Meer und in Gewassern. *Handbuch der Geophysik*, Vol. 7, Springer, 723–768.

Martin, D. W., and D. N. Sikdar, 1975: A case study of Atlantic cloud clusters: Part 1. Morphology and thermodynamic structure. *Mon. Wea. Rev.*, **103**, 691–708.

——, and ——, 1979: A case study of west Atlantic cloud clusters: Part 2. Dynamic structure and environment. *Mon. Wea. Rev.*, **107**, 1343–1369.

Monahan, E. C., 1971: Oceanic whitecaps. *J. Phys. Oceanogr.*, **1**, 139–144.

Patterson, E., D. Gillette and B. H. Stockton, 1977: Complex index of refraction between 300 and 700 nm for Saharan aerosols. *J. Geophys. Res.*, **82**, 3153–3161.

Payne, R. E., 1972: Albedo of the sea surface. *J. Atmos. Sci.*, **29**, 959–969.

Prospero, J. M., 1979: Dust from the Sahara. *Natural History*, **88**, p. 54ff.

Smith, E. A., and D. R. Phillips, 1972: Automated cloud tracking using precisely aligned digital ATS pictures. *IEEE Trans. Comput.*, **C-21**, 715–721.

——, and D. Loranger, 1977: Radiometric calibration of polar and geosynchronous satellite shortwave detectors for albedo measurements. Dept. of Atmospheric Science, Colorado State University, Fort Collins (unpublished manuscript).

Volz, F. E., 1970: Spectral skylight and solar radiance measurements in the Caribbean: Maritime aerosols and Sahara dust. *J. Atmos. Sci.*, **27**, 1041–1047.